Spin-wave transmission through an internal boundary: Beyond the scalar approximation

Roman Verba,[1] Vasil Tiberkevich,[2] and Andrei Slavin[2]
[1]*Institute of Magnetism, Kyiv 03142, Ukraine*
[2]*Department of Physics, Oakland University, Rochester, Michigan 48309, USA*

(Received 15 January 2020; revised manuscript received 25 March 2020; accepted 27 March 2020; published 20 April 2020)

The transmission and reflection of a spin wave at an internal boundary created by the local variation of anisotropy (or a bias magnetic field) are studied taking into account not only the changes in the wave amplitude, but also the changes in the wave polarization. It is shown that the account of the changes in the spin-wave polarization before and after the boundary leads to (i) increase of the spin-wave amplitude reflection coefficient, (ii) appearance of an additional phase shift $\Delta\phi \neq 0, \pi$ in both transmitted and reflected waves, and (iii) creation of additional evanescent waves in the vicinity of the boundary. It is also shown that even when significant changes in the transmitted wave polarization take place at the boundary, a spin wave could pass a finite-width boundary without reflection, if a certain resonance condition is satisfied. The effect of the polarization change at an internal boundary is especially pronounced for the exchange-dominated spin waves, while in the case of the dipole-dominated spin waves, this effect can vanish completely for certain configurations of the static magnetization.

DOI: 10.1103/PhysRevB.101.144430

I. INTRODUCTION

Spin waves (SWs) in ferromagnetic materials are considered as promising candidates for signal carriers in the next generation of signal processing devices. This is closely related to the attractive intrinsic properties of spin waves, such as relatively low damping, high frequency, small wavelength, down to tens of nanometers, and a variety of possible nonlinear SW interactions [1–5]. In order to process information, one should be able to perform different linear and nonlinear operations with SWs. In particular, the operations of interest for signal processing are controllable reflection/transmission of SWs and variation of the SW phase, which can be performed by a local variation of the SW spectrum. Such local spectrum variations were realized many times in bulk and submillimeter ferromagnetic (FM) samples by the application of an additional localized static magnetic field. In particular, attenuation [6,7] and frequency-dependent reflection [8] of SWs by a field-induced inhomogeneity were realized, as well as the resonance tunneling of SWs through a potential barrier [9], and generation of SW pulse trains by magnetic field-induced mirrors [10].

At nanoscale, however, application of local (10–100 nm) magnetic field is technically complicated and inefficient. Instead, it is much more convenient and energy efficient to vary the local magnetic properties of the propagation medium using a variety of magnetoelectric effects [11–14], among which one of the most promising for application at a nanoscale is the effect of voltage-controlled magnetic anisotropy (VCMA) in ferromagnetic metal/dielectric heterostructures [15–17]. The use of the VCMA effect has been already proposed for magnetic recording [18,19], excitation of SWs [20–23] and magnetic solitons [24]. In the VCMA effect, as well as in several other magnetoelectric effects, the application of an electric field results in the variation of the FM *magnetic anisotropy* which, of course, leads to the variation of the SW spectrum [25,26].

It is important to note that SWs are characterized not only by their dispersion relation, but also by the vector structure. Magnetization precession is circular only in an isotropic ferromagnetic sample. The presence of crystalline or shape anisotropy, as well as dynamic dipolar interaction, which is anisotropic, leads to an elliptic trajectory of the magnetization precession, i.e., to the appearance of a nonzero SW ellipticity $\varepsilon = 1 - m_{\min}/m_{\max}$, where $m_{\min,\max}$ are the dynamic magnetization components in the propagating SW. As the SW ellipticity is determined by the total effective anisotropy, the variation of the material anisotropy in the propagation medium, caused, e.g., by an external bias electric field through the VCMA effect, could *significantly* modify the ellipticity of a propagating SW. Strictly speaking, the application of a localized external static magnetic field also changes the SW ellipticity, except in some symmetric cases (like the case of SW propagation in the perpendicularly magnetized isotropic FM film), because it changes the relation between the components of total effective magnetic field acting on the magnetization. However, this effect is much weaker, than the effect of the local anisotropy variation.

This is illustrated by Fig. 1, where the SW spectra and ellipticity are shown for SWs propagating in an in-plane magnetized FM nanowire subjected to different in-plane bias magnetic fields [Figs. 1(a) and 1(c)] and different perpendicular electric fields [Figs. 1(b) and 1(d)], which modify the local magnetic anisotropy due to the VCMA effect. One can see, that in this example the parameters of the applied static magnetic and electric fields were chosen in such a way, that the SW spectral variations caused by the application of these fields were very similar. At the same time, the variation of

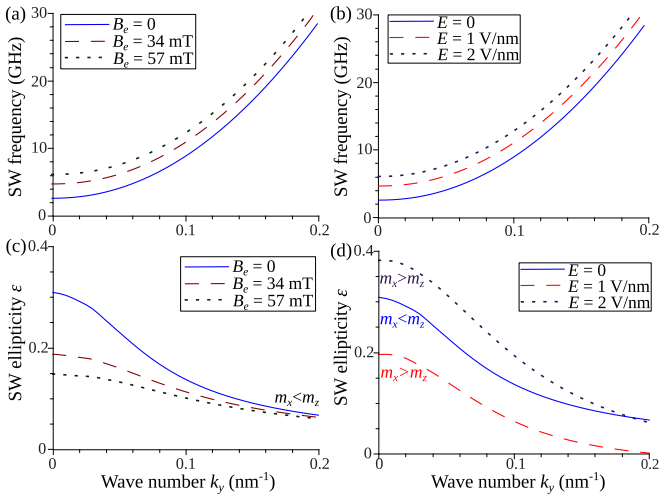

FIG. 1. Spectrum [(a) and (b)] and ellipticity [(c) and (d)] of SWs propagating in a ferromagnetic nanowire under different applied static magnetic fields [(a) and (c)] and electric fields, causing the local anisotropy modification via VCMA effect [(b) and (d)]. Parameters: Fe/MgO nanowire of the 20 nm width, Fe thickness 0.86 nm, static magnetization and the bias magnetic field are directed along the nanowire, saturation magnetization $M_s = 2.1$ T, exchange length $\lambda_{ex} = 3.4$ nm, constant of the perpendicular surface anisotropy $K_s = 1.36$ mJ/m^2, and magnetoelectric coefficient $\beta = 100$ fJ/(Vm) [27].

the SW ellipticity in the case of the anisotropy modification caused by the electric field are much more pronounced. With the anisotropy modification, the ellipticity variation takes place in a wider range of the SW wave numbers, and even the major and minor axes of the magnetization precession in the propagating SW could be interchanged by the action of the external electric field through the VCMA effect [see Fig. 1(d)].

Thus it is only natural to ask a question on how such a significant modification of the SW vectorial structure would affect the transmission and reflection of SWs from the internal boundary created by the local variation of the FM anisotropy, and under which circumstances this effect becomes practically important.

Theoretically the problem of SW transmission between different ferromagnetic materials or different regions of the same material was studied for many years. Starting from seminal work by Rado and Weertman [28] there were many research interest to the boundary conditions at the ferromagnet interface, including study of the effect of magnetoelastic interaction [29], finite width and diffusive character of interfaces [30–32], nonuniform dipolar fields [33,34], Dzyaloshinski-Moriya interaction [35], magnetic anisotropy of interface [36,37], etc. The problem of the SW reflection from a sharp boundary was studied in details for exchange-dominated SWs in isotropic, uniaxial and biaxial anisotropic ferromagnets [38–40]. The case of smooth interface was studied for both dipolar [6,7] and exchange-dominated SWs [30,31]. A closely related problem of the phase accumulation of SWs propagating in a nonuniform field was considered in Refs. [41,42]. Recently, the problem of transmission and reflection of exchange-dominated SWs from an interface between two biaxial magnetic materials has been considered again [43] and formation of surface exchange SWs at the boundary has been predicted for the first time.

In almost all the previously published papers, the problem of the SW transmission through a boundary (or a region with modified magnetic parameters) was considered within a scalar approximation, in which SW was described by a single effective scalar variable. This scalar variable can be introduced in a multiple ways. Either a spin density formalism can be employed [38,39] or a single variable describing circularly polarized dynamic magnetization can be introduced [41] or one of the dynamic magnetization components is simply neglected [6,7].

In our current work, we go beyond the scalar approximation and study the SW transmission and reflection using the full *vector* equations of motion, accounting, thus, for the SW *polarization*. As it will be shown below, the variation of the SW polarization results in a qualitatively different behavior of a SW transmitted through a boundary, such as the appearance of localized modes near the boundary, and appearance of a nonzero phase shift in the transmitted wave. We develop an analytical theory of the SW transmission through a sharp internal boundary for dipole-exchange and exchange-dominated SWs, and derive a criterion allowing one to determine the range of validity of the commonly used scalar approximation. The developed theory is general, and is not limited to the case when the internal boundary is introduced by the VCMA. This case will be discussed below simply to illustrate the developed general formalism.

The paper is organized as follows. In Sec. II, the geometry of the problem, and the general equations of motion for the magnetization are introduced. The boundary conditions, and the vectorial structure of SWs modes, localized near the boundary, are described in Sec. III. Analytical expressions for the coefficients of SW transmission and reflection from an isolated boundary, and from a finite-width region with modified magnetic parameters (two consequent boundaries separated by a finite distance) are derived and discussed in Sec. IV within the exchange approximation. Effects of the dipolar interaction on the obtained results are discussed in Sec. V. Finally, conclusions are given in Sec. VI.

II. MODEL AND INITIAL EQUATIONS

The geometry of the considered problem is shown in Fig. 2. We consider a quasi-one-dimensional problem, when SWs propagate in a ferromagnetic waveguide (e.g., stripe or nanowire) along the axis of a waveguide (y axis in Fig. 2). The boundary between the regions with different magnetic properties is perpendicular to the SW propagation direction (x-axis). We also assume that the SW profile in the x-z plane (perpendicular to the propagation direction) remains unchanged in both regions. This assumption is absolutely natural for relatively thin ferromagnetic films and nanowires with the thickness of the order of several exchange lengths for a given FM material. In such a case, the SW profile along the film thickness is maintained uniform by the exchange interaction, and the width profiles of different SW modes are defined by

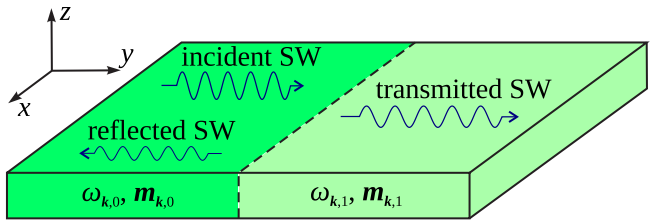

FIG. 2. Geometry of an SW waveguide with a single internal boundary: SW propagates along the FM waveguide through a sharp internal boundary between the two waveguide regions which have different magnetic properties, and, therefore, different SW dispersion relations and different vector structure (polarization) of the SW modes.

the effective dipolar boundary conditions, which are almost independent of the SW wave vector and values of the bias magnetic field or anisotropy [33,34,44]. The assumption of a constant SW transverse profile works also in much larger samples, like micrometer-sized ferromagnetic strips or films, if the propagation of the *bulk* SW modes is considered. For example, such a case is realized if a FM film or a strip is magnetized in the y or z directions. A well-known exemption, which cannot be considered within the above mentioned assumption, is the Damon-Eshbach surface SW mode, which propagates in an in-plane magnetized film perpendicularly to the direction of the static magnetization (i.e., the static magnetization is along the x direction in Fig. 2). The thickness profile of the Damon-Eshbach mode depends on its wave number [45] (in relatively thick films), and the solution of the boundary problem in such a case requires accounting of *all* the SW modes of the film.

We consider the SW propagation in an FM waveguide through an internal boundary—a boundary between two regions of the same FM waveguide. This boundary can be created by any external influence, e.g., by the application of an external bias magnetic field, electric field or strain. Thus the regions of the FM waveguide separated by the boundary can differ by the values of the static internal magnetic field or magnetic anisotropy, while the saturation magnetization M_s and the exchange length $\lambda_{\rm ex}$ are the same in both regions. The static magnetization is assumed to be uniform, and have the same direction in both separated regions of the waveguide. The boundary is considered to be sharp, which physically means that the area in which the external control parameter (magnetic field, electric field, strain, etc.) varies is much smaller tnan the SW wavelength. For ultrathin nanowires, where the magnetic anisotropy could be modified by the VCMA effect, this is an absolutely natural approximation for all the range of the experimentally achievable SW wavelengths. It should be noted, that below we do not use any specific features of VCMA-induced anisotropy variation. All the theory uses only the SW dispersion relation and vector structure, and, thus, could be applied to boundaries created by any physical effects within the limits described above. Also, the theory can be generalized to the case of the interface between the *different* ferromagnetic materials, and one should expect qualitatively similar effects.

Within the above formulated approach the propagation of SWs is described by the following equation (see Refs. [46–48] for the details of this formalism):

$$\frac{\partial \boldsymbol{m}(y,t)}{\partial t} = \boldsymbol{\mu} \times \hat{\boldsymbol{\Omega}} * \boldsymbol{m}(y',t)\,, \tag{1}$$

where the tensor operator

$$\hat{\boldsymbol{\Omega}} = \delta(y-y')\left(\gamma B - \omega_M \lambda_{\rm ex}^2 \frac{\partial^2}{\partial y^2} + \omega_M \hat{\boldsymbol{N}}_{\rm an}\right) + \omega_M \int dy' \hat{\boldsymbol{G}}_{\rm dip}(y-y'). \tag{2}$$

Here, $\boldsymbol{\mu}$ ($|\boldsymbol{\mu}| = 1$) and $\boldsymbol{m}(y,t)$ are the dimensionless static and dynamic magnetization components, so that the full magnetization vector is written as $\boldsymbol{M}(y,t) = M_s(\boldsymbol{\mu} + \boldsymbol{m}(y,t))$, B is the static internal magnetic field inside the FM waveguide, $\lambda_{\rm ex}$ is the exchange length of the FM material, tensor $\hat{\boldsymbol{N}}_{\rm an} = -B_{\rm an}/(\mu_0 M_s)(\boldsymbol{e}_{z'} \otimes \boldsymbol{e}_{z'})$ describes the uniaxial anisotropy with effective anisotropy field $B_{\rm an}$ and anisotropy axis $\boldsymbol{e}_{z'}$ [47], and $\hat{\boldsymbol{G}}_{\rm dip}$ is the magnetostatic Green's function, which depends on the sample geometry [49]. For the considered problem, obviously, B and $\hat{\boldsymbol{N}}_{\rm an}$ can be different in different regions of the FM waveguide. Since the magnetic damping is not of a qualitative importance for the particular scattering problem considered here, in the following it is neglected. Note, that if the profile of the propagating SW mode is not uniform in the x-z plane, Eq. (2) remains valid, but proper expression for the Green's function $\hat{\boldsymbol{G}}_{\rm dip}$ should be used (i.e., when averaging standard two-dimensional Green's function over the nanowire width actual SW profile should be taken into account [49]).

Considering transmission of a monochromatic SW with the angular frequency ω, we represent the SW dynamic magnetization via its complex amplitudes: $\boldsymbol{m}(y,t) = (\boldsymbol{m}(y)\exp[-i\omega t] + \text{c.c.})$, which results in the replacement $\partial \boldsymbol{m}(y,t)/\partial t \to -i\omega \boldsymbol{m}(y)$ in Eq. (1). In a general case, the resulting integral-differential equation can not be solved analytically. However, for a sufficiently large SW wave number k (see criteria below), the exchange interaction becomes dominant, and the integral operator in Eq. (2) can be replaced with its Fourier-transform $\hat{\boldsymbol{F}}_k = \int \hat{\boldsymbol{G}}_{\rm dip}(y) e^{-iky} dy$. Consequently, Eq. (1) becomes an ordinary differential equation, which for the considered case of a sharp boundary can be solved in each region separately, and a proper boundary conditions should be applied. In both regions separated by the boundary, the SW has the form of a harmonic wave with the wave vector $\boldsymbol{k} = k\boldsymbol{e}_y$: $\boldsymbol{m}(y,t) = (\boldsymbol{m}_k \exp[i(ky - \omega_k t)] + \text{c.c.})$. The SW dispersion relation $\omega_k(k)$ and the vector structure $\boldsymbol{m}_k$ of the propagating SW mode are determined from the following eigenvalue problem [46,47]:

$$-i\omega_k \boldsymbol{m}_k = \boldsymbol{\mu} \times \hat{\boldsymbol{\Omega}}_k \cdot \boldsymbol{m}_k\,, \tag{3}$$

$$\hat{\boldsymbol{\Omega}}_k = \left(\gamma B + \omega_M \lambda_{\rm ex}^2 k^2\right)\hat{\boldsymbol{I}} + \omega_M(\hat{\boldsymbol{F}}_k + \hat{\boldsymbol{N}}^{\rm an})\,. \tag{4}$$

The range of validity of the above described exchange approximation can be easily evaluated from Eqs. (3) and (4). Comparing the exchange contribution to the SW energy (frequency) and maximal possible dipolar contributions one finds that the last one is negligible if $\lambda_{\rm ex}^2 k^2 \gg \max_{\alpha,\beta} |F_{k,\alpha\beta} - F_{0,\alpha\beta}|$. Note that $\hat{\boldsymbol{F}}_0$ is the simple static demagnetization tensor of the used FM waveguide.

III. BOUNDARY CONDITIONS AND EVANESCENT SPIN WAVES

In the case when $\boldsymbol{M}_0$ and λ_{ex} are the same in both regions, the following conditions of continuity of the dynamic magnetization $\boldsymbol{m}(y)$ and its derivative should be satisfied at the boundary (located at $y = 0$):

$$\boldsymbol{m}(y = 0_-) = \boldsymbol{m}(y = 0_+), \quad \left.\frac{\partial \boldsymbol{m}}{\partial y}\right|_{y=0_-} = \left.\frac{\partial \boldsymbol{m}}{\partial y}\right|_{y=0_+}. \quad (5)$$

If the SW vector structure is the same in both regions, one can represent dynamic magnetization using a scalar variable $a(y)$: $\boldsymbol{m}(y) = \boldsymbol{m}_0 a(y)$. In such a scalar approximation, the conditions (5) are reduced to two scalar equations, and it is easy to calculate the SW reflection R and transmission T coefficients at the boundary by choosing the solution as a sum of incident and reflected waves before the boundary, $a(y < 0) = e^{ik_0 y} + Re^{-ik_0 y}$, and a single transmitted wave after the boundary, $a(y > 0) = Te^{ik_1 y}$. This solution is well-known

$$R = \frac{k_0 - k_1}{k_0 + k_1}, \quad T = \frac{2k_0}{k_0 + k_1}. \quad (6)$$

The wave number k_1, of course, is determined form the dispersion relation, so that the frequencies of the incident and transmitted SWs are the same: $\omega_0(k_0) = \omega_1(k_1)$. From Eq. (6), it is clear that the SW reflection coefficient increases when the difference of SW wave numbers, determined by the difference of the external control parameters before and after the boundary becomes larger. One can also see, that the transmitted SW is always in phase with the incident one, while the reflected SWs could be in phase, or acquire a phase shift $\Delta\phi = \pi$ depending whether $k_0 > k_1$ or not.

In a general "vectorial" case, however, one should use the full boundary conditions (5). It is clear, that choosing solution as a sum of the incident and reflected SWs before the boundary and as a single transmitted SW after the boundary, it is not possible to satisfy the boundary conditions as there are only two scalar parameters to be determined (R and T) and four scalar equations to be satisfied (since $\boldsymbol{m}$ is, effectively, a two-component vector perpendicular to the static magnetization). Consequently, there should be the *other* waves, which, together with the incident, reflected and transmitted SWs, will allow us to satisfy the boundary conditions.

To understand what are these "other" additional SWs, let us look closer at Eq. (3). For a fixed SW frequency ω, Eq. (3) can be considered as an eigenvalue problem for the SW wave vector k^2 and the vector $\boldsymbol{m}_k$ characterizing the vectorial structure of the SW mode. In the range of existence of the propagating SW mode this eigenvalue problem has two solutions: one with the $k^2 > 0$, which describes the propagating SWs having the vectorial profile $\boldsymbol{m}_k$, and the second solution with $k^2 = -\kappa^2 < 0$, which corresponds to the *exponentially localized (evanescent)* SWs with the spatial distribution $\boldsymbol{m}(y) \sim \exp[\pm\kappa y]$. The "wave number" of these evanescent SWs for an arbitrary anisotropy and static magnetization can be represented as

$$\kappa^2 = \frac{2\omega_k |\boldsymbol{m}_k|^2}{\omega_M \lambda_{ex}^2 A_k} - k^2, \quad (7)$$

where $A_k = i(\boldsymbol{m}_k^* \cdot \boldsymbol{\mu} \times \boldsymbol{m}_k)$ is the norm of the propagating SW mode $\boldsymbol{m}_k$ [46]. The vector structure of these localized waves (to the accuracy of an arbitrary multiplier) is determined as

$$\boldsymbol{m}_{ev} = \boldsymbol{\mu} \times \boldsymbol{m}_k^*. \quad (8)$$

For example, if a propagating SW has polarization $\boldsymbol{m}_k = m_x \boldsymbol{e}_x + i m_y \boldsymbol{e}_y$, then the structure of the evanescent SW is described by $\boldsymbol{m}_{ev} = m_y \boldsymbol{e}_x - i m_x \boldsymbol{e}_y$. In other words, the evanescent wave has the opposite direction of the magnetization vector rotation compared to the incident SW, and the precession ellipse in the case of an evanescent wave is rotated on 90°. Note that in a general case the polarizations of the propagating incident and the localized evanescent SWs are *orthogonal*, in the sense $\boldsymbol{m}_{ev}^* \cdot \boldsymbol{m}_k = 0$, that is expected. The existence of the similar evanescent SWs near the boundary was first predicted in Ref. [43].

The existence of these evanescent SWs is natural. The SWs with orthogonal polarization cannot propagate in a FM waveguide. Consequently, if such an SW is injected into the waveguide, it should decay at a certain decay length. Equation (7) determines the magnitude of the characteristic decay length $l = 1/\kappa$ of these evanescent SWs. It can be shown that $\kappa^2 > k^2$ for any parameters of the waveguide, i.e., the evanescent SW decays on the length which is of the order, or smaller, than the wavelength of the propagating SW of the same frequency.

IV. TRANSMISSION AND REFLECTION OF THE SPIN WAVES AT A BOUNDARY IN THE EXCHANGE APPROXIMATION

A. Single internal boundary

In this section, we calculate the transmission and reflection coefficients for a SW passing through a single internal boundary, as shown in Fig. 2. As it was pointed out in the previous section, for the proper description of scattering from the boundary one should represent the dynamical magnetization before the boundary as a sum of incident, reflected, and evanescent SWs:

$$\boldsymbol{m}(y < 0) = \boldsymbol{m}_{k,0}(e^{ik_0 y} + Re^{-ik_0 y}) + C_1 \boldsymbol{m}_{ev,0} e^{\kappa_0 y}, \quad (9)$$

and the magnetization after the boundary as a sum of a transmitted and another evanescent SWs:

$$\boldsymbol{m}(y > 0) = T\boldsymbol{m}_{k,1} e^{ik_1 y} + C_2 \boldsymbol{m}_{ev,1} e^{-\kappa_1 y}. \quad (10)$$

The amplitude of the incident propagating SW is assumed to be equal to 1. Substituting these equations for the wave amplitudes into the boundary conditions (5), one obtains four linear equations for the coefficients R, T, C_1, and C_2, which can be solved by well-known methods.

An example of the SW profiles (9) and (10) calculated using the full vectorial approach is presented in Fig. 3(b), and, for comparison, the similar profiles calculated within the traditional scalar approximation are presented in Fig. 3(a). For clarity, we have chosen the parameters of the scattering problem in such a way, that the incident and reflected SWs are circularly polarized (dynamic magnetization components $|m_x| = |m_z|$), while the transmitted SW has the elliptical polarization. In Fig. 3(b), one can clearly see the influence of

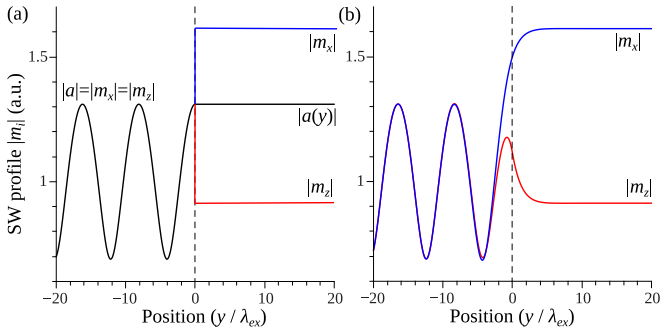

FIG. 3. Profiles of an SW mode near the boundary of two regions with different dispersion relation and different SW polarizations: (a) scalar approximation [Eq. (6)] and (b) full vectorial solution. Figures show the profiles of both components of the SW dynamical magnetization and, also, the profile of the effective scalar variable $a(y)$ [in (a) only]. The position of the boundary is shown by a vertical dashed line. Calculation parameters: $\lambda_{ex}k_0 = 0.39$, $\boldsymbol{m}_{k,0} = [1, 1]$, and $\lambda_{ex}k_1 = 0.2, \boldsymbol{m}_{k,1} = [1.77, 1]$ (which correspond to an FM waveguide magnetized in the y direction by the bias magnetic field $B_e = 0.1\mu_0 M_s$, isotropic in the zeroth region, and having perpendicular hard-axis anisotropy in the first region $N^{(an)}_{zz,1} = 0.3$. The SW frequency is $\omega = 0.25\omega_M$).

the localized evanescent SWs, which allow the components of the dynamic magnetization to vary continuously across the boundary. In contrast, in the scalar approximation Fig. 3(a), only the effective scalar parameter $a(y)$ (e.g., spin density) is continuous, while dynamic magnetization components have an unphysical discontinuity at the boundary. The oscillations before the boundary are caused by the interference of the incident and reflected SWs. We would like to note that the localization length of the evanescent SWs does not depend on the polarization difference in the two regions, and that these waves always appear if any polarization difference exists.

The transmission and reflection coefficients in the vectorial formalism have the following form:

$$T = \frac{2k_0(\kappa_0+\kappa_1)|\boldsymbol{m}_{k,0}|^2/(\boldsymbol{m}^*_{k,0}\cdot\boldsymbol{m}_{k,1})}{(k_0+k_1)(\kappa_0+\kappa_1) - i\mathcal{E}^2_{01}(k_0+i\kappa_1)(k_1+i\kappa_0)}, \quad (11a)$$

$$R = \frac{(k_0-k_1)(\kappa_0+\kappa_1) - i\mathcal{E}^2_{01}(k_0-i\kappa_1)(k_1+i\kappa_0)}{(k_0+k_1)(\kappa_0+\kappa_1) - i\mathcal{E}^2_{01}(k_0+i\kappa_1)(k_1+i\kappa_0)}. \quad (11b)$$

Here the quantity $\mathcal{E}_{01}$ is defined as

$$\mathcal{E}_{01} = \left|\frac{\boldsymbol{m}_{k,0}\cdot\boldsymbol{\mu}\times\boldsymbol{m}_{k,1}}{\boldsymbol{m}^*_{k,0}\cdot\boldsymbol{m}_{k,1}}\right|. \quad (12)$$

This quantity serves as a natural *measure of difference in the SW polarization* $\boldsymbol{m}_{k,0}$ and $\boldsymbol{m}_{k,1}$. In particular, it is equal to zero, if $\boldsymbol{m}_{k,0} = \boldsymbol{m}_{k,1}$, and $\mathcal{E} \to \infty$ for almost orthogonal SW polarizations when $\boldsymbol{m}^*_{k,0}\cdot\boldsymbol{m}_{k,1} \to 0$.

It is clear that for identical SW polarizations, when $\mathcal{E}_{01} = 0$, the vectorial expressions for the SW transmission and reflection coefficients (11) are reduces to Eq. (6), obtained in the scalar approximation. Inequality of the SW polarizations before and after the boundary leads to an increase of the SW reflection from the boundary, and a consequent decrease of the SW transmission. Additionally, it leads to the appearance of the phase shifts in both the reflected and transmitted waves

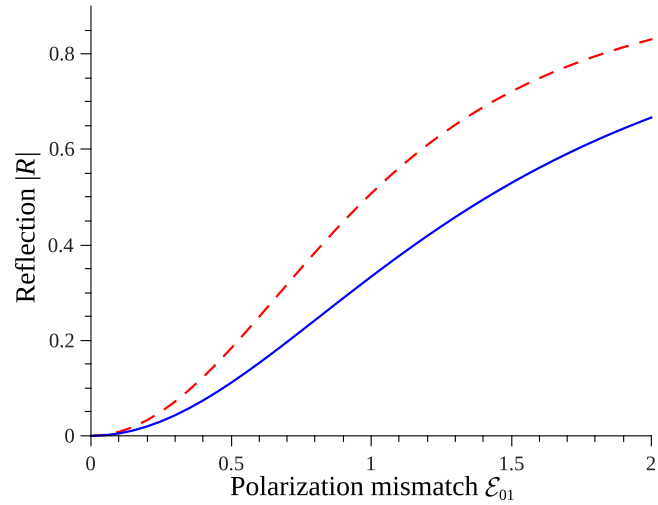

FIG. 4. Dependence of the SW reflection coefficient on the SW polarization mismatch for the case of identical SW wave numbers, but different vector structure of the SWs before and after the boundary: solid line – $\kappa = k$ and dashed line – $\kappa = 3k$.

relative to the incident one, which can take any value $\Delta\phi \in [-\pi, \pi]$ (recall that in the scalar approximation $\Delta\phi = 0, \pi$ for the reflected wave, and there is now phase shift for the transmitted wave). It is important to note that even if the SW wave vectors are identical, the SW would not be fully transmitted through the boundary if the polarization mismatch exists: $T \neq 1$, $R \neq 0$ for $k_0 = k_1$, and $\mathcal{E}_{01} \neq 0$. Finally, it is interesting to note that for a large SW polarization difference ($\mathcal{E}_{01} \gg 1$) the transmission coefficient is reduced to zero, $T \to 0$, while the reflection coefficient approaches the value:

$$R \to \frac{k_0 - i\kappa_1}{k_0 + i\kappa_1}, \quad (13)$$

which coincides with Eq. (6), obtained in the scalar approximation, assuming that the only SW existing after the boundary is the evanescent one, having the inverse localization length κ_1. Naturally, $|R| \to 1$ in this case.

Let us now look quantitatively at the influence of the SW polarization mismatch on the SW reflection and transmission coefficients. For this purpose, we calculate the R and T coefficient for a model system, assuming that the SW wave numbers in both regions are the same, $k_0 = k_1$ and $\kappa_0 = \kappa_1$, while the polarization difference $\mathcal{E}_{01}$ is nonzero. In this case, the SW reflection is caused only by the SW polarization difference. Such a situation is not just an abstract theoretical model, but it can be realized, for example, at the interface between the FM waveguides having the same anisotropy field, but the anisotropy axes that are perpendicular to each other.

The calculated dependencies of the SW reflection coefficient $|R|$ are shown in Fig. 4. As one can see, the effect of the polarization mismatch on the SW reflection and transmission depends, also, on the ratio of the SW wave number k to the inverse localization length of the corresponding evanescent wave κ; for a larger ratio κ/k, the reflection is stronger.

This can be easily understood by recalling, that in the well-known scalar case the reflection is proportional to

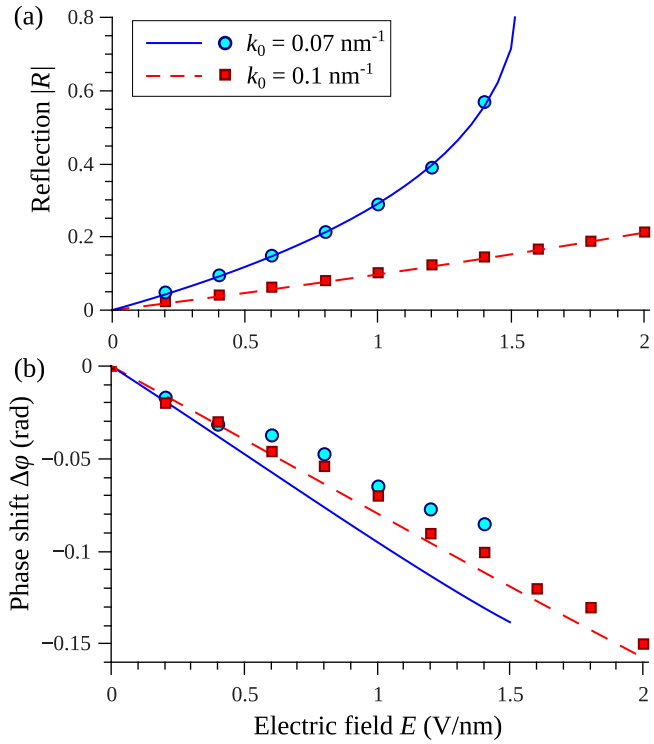

FIG. 5. Dependence of the SW reflection coefficient (a) and the phase shift of the reflected SW (b) on the control parameter (electric field applied in the region after the boundary) for different wave number of the incident SW; lines: theory and symbols: results of micromagnetic simulations. The material and geometrical parameters are as in Fig. 1.

the difference of the wave vectors of between the incident and the transmitted waves. Similarly, in our case when the difference in characteristic scales of the incident and the localized waves increases, a greater part of the incident SW is reflected from the boundary. As it was pointed out earlier, $\kappa^2 \geqslant k^2$ for any stable magnetic configuration, and the ratio κ/k increases with the increase of the band gap in the SW spectrum (i.e., with the increase of the value ω_0).

It should be noted that the influence of the polarization mismatch on the reflection is proportional to $\mathcal{E}_{01}^2$, and, consequently, it is almost unnoticeable for the small polarization difference ($\mathcal{E}_{01} < 0.1$–0.2 in Fig. 4). Obviously, when the SW wave vectors are also different, which results in a nonzero reflection for $\mathcal{E}_{01} = 0$, the effect of the polarization mismatch on the amplitude of the reflected wave will be pronounced only for even higher values of $\mathcal{E}_{01}$.

As an example, in Fig. 5, we calculated the reflection coefficient $|R|$ and the phase shift $\Delta\phi$ of an SW reflected in an ultrathin nanowire where the sharp internal boundary was created by an external electric field via VCMA, so the perpendicular magnetic anisotropy was changed at the boundary. As it was shown in Fig. 1, the SW polarization can significantly change in such a case, resulting in the polarization mismatch up to $\mathcal{E}_{01} = 0.3$ in the studied range of applied electric field values. We found that the difference between the values of the reflection coefficient $|R|$ in the full vectorial solution Eq. (11) and in the scalar approximation Eq. (6) does not exceed 1%.

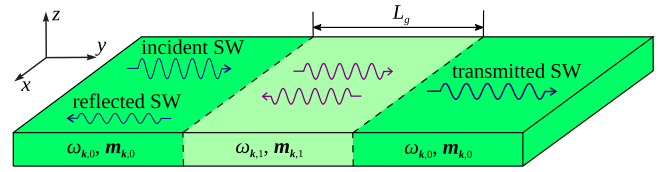

FIG. 6. Geometry of an SW waveguide with two internal boundaries: SW in the course of propagation in an FM waveguide encounters a region of a finite length L_g with different magnetic parameters

However, at the same time one can clearly see in Fig. 5 an additional phase shift in the reflected SW up to 0.15 rad, which could be easily detected and should be taken into account in the design of SW signal processing devices.

We have also verified our theoretical calculations by micromagnetic simulations using MuMax3 micromagnetic solver [50]. In these simulations, we set the nanowire length to 4 μm, SWs are exited by a local, 50 nm in length, application of microwave magnetic field b_z of the magnitude $b_z = 0.1$ mT and the frequency of 5.52 GHz (corresponding to $k_0 = 0.07$ nm^{-1}) and 8.85 GHz ($k_0 = 0.1$ nm^{-1}), and the internal boundary is separated by 1 μm from the excitation source. To increase the precision of the determination of reflected wave amplitude and phase, the damping rate is set to $\alpha_G = 10^{-4}$, except for the regions near the nanowire beginning and end, where it increases quadratically, which ensures absence of SW reflections form these edges. The complex reflection coefficient R is extracted from the magnetization dynamics in the region between the excitation area and internal boundary (but not close to the boundary, so that evanescent waves become negligible), by its fitting by the sum of incident and reflected waves.

As one can see in Fig. 5, the modulus of the reflection rate $|R|$ is nicely reproduced by micromagnetic simulations. In the case of shorter incident SW having $k_0 = 0.1$ nm^{-1}, our theory predicts well also the phase shift of the reflected wave. In the case of longer incident SW, $k_0 = 0.07$ nm^{-1}, we also see clear additional phase shift of the reflected SWs, induced by the polarization mismatch, however, this shift is somewhat smaller than predicted one. The reason of this discrepancy is the increased role of the dipolar interaction in the propagation of longer SWs, which is discussed in more details in Sec. V.

Thus, we can conclude that the SW polarization mismatch before and after the boundary leads to three main effects. The first one, which is clearly visible for any polarization mismatch, is the appearance of the localized evanescent SWs at the boundary. The second effect is the additional phase shift for both reflected and transmitted SWs. Finally, the third one is a decrease of the transmission and increase of reflection coefficients which, however, is measurable only for sufficiently large values of the polarization mismatch $\mathcal{E}_{01}$.

B. Finite region with different SW dispersion and polarization

In this section, we consider the SW scattering from a region ("gate") of a finite gate length L_g, inside which the magnetic parameters (magnetic field or anisotropy) of a waveguide are modified (see Fig. 6). Such structures can be used for the effective control of the phase and amplitude of a propagating SW in the SW-based signal processing. In experiment, such

a geometry can be realized by applying a control voltage in a spatially extended region of the SW waveguide (middle region in Fig. 6).

Within a standard scalar approximation the solution of this transmission problem is well-known, and the transmission coefficient T is given by

$$|T|^2 = \left[1 + \frac{1}{4}\left(\frac{k_0}{k_1} - \frac{k_1}{k_0}\right)^2 \sin^2(k_1 L_g)\right]^{-1}. \qquad (14)$$

The reflection coefficient can be calculated from the equality $|T|^2 + |R|^2 = 1$. Of course, this solution is valid if the gate length L_g is significantly smaller, than the SW mean free path.

For the calculation of the transmission coefficient within the full vectorial approach one should take into account an incident ($e^{ik_0 y}$), reflected ($Re^{-ik_0 y}$), and one evanescent ($C_1 e^{\kappa_0 y}$) SW in the first region (left one in Fig. 6), two propagating ($C_2 e^{ik_1 y}$ and $C_3 e^{-ik_1 y}$) and two evanescent [$C_4 e^{-\kappa_1 y}$ and $C_5 e^{\kappa_1 (y - L_g)}$] SWs inside the middle (gate) region, and one transmitted propagating SW ($Te^{ik_0 (y - L_g)}$) and one evanescent SW ($C_6 e^{-\kappa_0 (y - L_g)}$) in the last (right) region. In this geometry, the positions of the sharp internal boundaries are assumed to be at $y = 0$ and L_g, respectively. By the application of two pairs of conditions Eq. (5) at both boundaries, one can obtain the amplitudes of all the propagating and evanescent waves. The exact solution of the problem is too cumbersome to be presented here. Thus below we will show only the solutions obtained in several most important particular cases.

To illustrate the qualitative influence of the polarization mismatch on the SW propagation through a gate of a finite length, we present below the dependence of the transmission coefficient on the gate length L_g for a model problem illustrated in Fig. 7 and compare it with the similar results obtained in the scalar approximation Eq. (14). The following features of the SW scattering from the finite-size gate can be seen from Fig. 7. First, the function $|T|^2(L_g)$ is still a periodic function, except in the case of small gate lengths, when the amplitudes of the evanescent SWs localized at one of the boundaries are not vanishing the other another boundary, i.e., when $\exp[\kappa_1 L_g]$ is not a negligible value. The period of the function $|T|^2(L_g)$ is the same as in the scalar approximation, and is equal to $2\pi/k_1$. Second, the minimum value of the transmission coefficient becomes smaller due to the influence of polarization difference. Finally, the most interesting feature is the fact, that the maximum value of transmission coefficient can be $\max |T|(L_g) = 1$, i.e., an SW can pass the gate region resonantly. This resonance transmission could appear to be rather surprising, since the SW passes two boundaries where a part of the SW polarization is lost. In a certain sense, this is an analog of the well-known resonance tunneling of particles in quantum mechanics, and the role of the tunnel barriers is played by the internal boundaries. The resonant transmission takes place if the condition $k_1 L_g + \psi = \pi n$, $n \in \mathbb{Z}$ is satisfied (see the definition of ψ below). In a scalar approximation, the resonant transmission also takes place, under the condition $k_1 L_g = \pi n$ (see Eq. (14) or Ref. [40]). The appearance of the phase ψ in the resonance conditions is related to the additional phase shift, which is acquired by an SW reflected from a boundary due to a nonzero polarization mismatch.

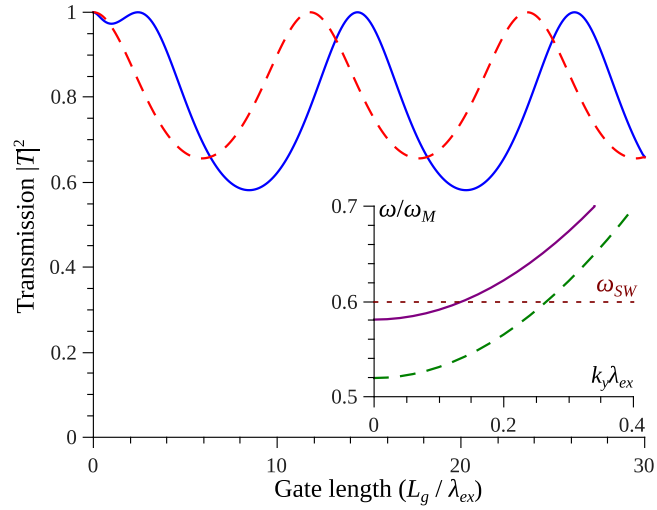

FIG. 7. Coefficient of SW transmission through a gate of a finite length L_g; solid lines: full vectorial solution and dashed lines: scalar approximation. Parameters: internal field $B/\mu_0 M_s = 0.1$, effective anisotropy tensor (including static demagnetization tensor) $N^{(an)}_{xx,1} = 0.8$, $N^{(an)}_{yy,1} = 0.2$ within the gate region, and $N^{(an)}_{xx,0} = 0.35$, $N^{(an)}_{yy,0} = 0.65$ outside this region, SW frequency $\omega_{SW} = 0.6\omega_M$. The corresponding SW spectra are shown in the inset, dashed line; within the gate region, solid: outside this region; for these parameters, the SW polarization difference is $\mathcal{E}_{01} = 0.37$.

An reasonably simple analytical expression for the SW transmission coefficient can be derived assuming that amplitude of the evanescent SW localized at one of the boundaries is vanishingly small at the other boundary, i.e., if $\exp[-\kappa_1 L_g] \ll 1$. Within this approximation the SW transmission coefficient can be written as

$$|T|^2 = \left[1 + \frac{1}{4}\left[\left(\frac{k_0}{k_1} - \frac{k_1}{k_0}\right)^2 + \mathcal{E}_{01}^2 f\right] \sin^2(k_1 L_g + \psi)\right]^{-1}. \qquad (15)$$

Here, f and ψ are the coefficients which depend on the SW wave numbers k_i, "wave numbers" κ_i of the localized evanescent waves, and the SW vector structure. In a general case, the explicit expressions for f and ψ are rather cumbersome, and we will not present them below. It is clear, that for a negligible difference of the SW polarization, $\mathcal{E}_{01} \ll 1$, the above presented equation is reduced to Eq. (14) ($\psi = 0$ for $\mathcal{E}_{01} = 0$, see below).

The expressions for f and ψ in a compact explicit form can be also derived in several limiting cases. For a small polarization mismatch, $\mathcal{E}_{01} \ll 1$ these expressions have the following form:

$$f = 2\frac{\left(k_0^2 - k_1^2\right)\left(k_0^2 \kappa_0 - k_1^2 \kappa_1\right)}{k_0^2 k_1^2 (\kappa_0 + \kappa_1)}, \qquad (16a)$$

$$\psi = \frac{1}{2}\arcsin\left[4\mathcal{E}_{01}^2 \frac{k_1\left(k_0^2 + \kappa_0\kappa_1\right)}{\left(k_0^2 - k_1^2\right)(\kappa_0 + \kappa_1)}\right]. \qquad (16b)$$

It is clear, that for $\mathcal{E}_{01} = 0$ the phase $\psi = 0$, as it was pointed out above. In particular, using Eq. (16), we can calculate the effect of the polarization mismatch on the SW transmission for a VCMA gate (all the parameters used are the

same as in Fig. 5). When the applied gate voltage $E = 2\,\mathrm{V/nm}$ the value $\mathcal{E}_{01}^2 f$ is only 4% of the polarization-independent term $(k_0/k_1 - k_1/k_0)^2$. Consequently, the minimum transmission coefficient also decreases by around 4%. The phase ψ which affects the condition of the resonance transmission through the finite-length gate is equal to $\psi = 0.15\,\mathrm{rad}$, which is not a negligible value, and should be taken into account.

Another limiting case, in which compact expressions for f and ψ can be derived, is the case of a large polarization mismatch, i.e., the case when $\mathcal{E}_{01} \gg 1$. In this limit, the coefficients in Eq. (15) can be calculated as

$$f = \mathcal{E}_{01}^2 \frac{\left(k_0^2 + \kappa_1^2\right)^2 \left(k_1^2 + \kappa_0^2\right)^2}{k_0^2 k_1^2 (\kappa_0 + \kappa_1)^4}, \tag{17a}$$

$$\psi = \frac{1}{2} \arcsin\left[\frac{4k_1\kappa_0\left(\kappa_0^2 - k_1^2\right)}{\left(\kappa_0^2 + k_1^2\right)^2}\right]. \tag{17b}$$

The case of a large polarization mismatch is, basically the case of a large ellipticity of the SW precession, for which typically $\kappa \gg k$. Consequently, one can see that in such a case $\psi \to 0$, similarly to the case of small values of $\mathcal{E}_{01}$.

V. EFFECT OF DIPOLAR INTERACTION

In the previous sections, we neglected the effect of the dynamic dipolar interaction on the SW propagation and transmission through an internal boundary. For a sufficiently short SWs and thin ferromagnetic films, this approximation is natural and correct. However, in the range of relatively small SW wave numbers the dynamic dipolar interaction becomes important, and, also, its influence is more pronounced in relatively thick ferromagnetic films.

The problem of transmission of dipole-exchange SWs through an internal boundary is a complex challenging task, which has not been solved analytically even within the scalar approximation. In order to understand main features of the SW transmission in the dipole-exchange case we, first, consider the case of purely dipolar SWs (magnetostatic waves), neglecting the exchange interaction. This approximation is valid if all the dimensions of a ferromagnetic waveguide and the SW wavelength are much larger than the exchange length in the waveguide FM material.

The propagation of the dipolar SWs is described by the Walker's equation [51] for magnetostatic potential ψ:

$$\mathrm{div}(\hat{\boldsymbol{\mu}} \cdot \nabla\psi) = 0, \tag{18}$$

where $\hat{\boldsymbol{\mu}} = \hat{\boldsymbol{\mu}}(\omega) = \hat{\boldsymbol{I}} + \hat{\boldsymbol{\chi}}$ is the tensor of magnetic permeability, and $\hat{\boldsymbol{\chi}}$ is the tensor of magnetic susceptibility. In the coordinate system where the z' axis is aligned along the direction of static magnetization the susceptibility tensor $\hat{\boldsymbol{\chi}}$ has only four nonzero components:

$$\hat{\boldsymbol{\chi}} = \frac{\omega_M}{\omega_0^2 - \omega^2} \begin{pmatrix} \omega_H + \omega_{\mathrm{an},y'} & i\omega & 0 \\ -i\omega & \omega_H + \omega_{\mathrm{an},x'} & 0 \\ 0 & 0 & 0 \end{pmatrix}, \tag{19}$$

where $\omega_{\mathrm{an},i} = \gamma B_{\mathrm{an},i}$, $B_{\mathrm{an},x'}$, and $B_{\mathrm{an},y'}$ are the anisotropy fields in the x' and y' directions (anisotropy is assumed to be biaxial), and $\omega_0^2 = (\omega_H + \omega_{\mathrm{an},x})(\omega_H + \omega_{\mathrm{an},y})$ is the ferromagnetic resonance frequency in the waveguide.

In order to make the calculations simple and clear, we consider a metalized FM waveguide where the static magnetization direction is along the z axis (the case of a perpendicularly magnetized waveguide). The coordinate system is the same as the one shown in Fig. 2. In this case from the boundary conditions at the metalized surfaces, which require $(\hat{\boldsymbol{\mu}}\nabla\psi)_z = 0$, one gets a profile of the dipolar SW eigenmodes: $\psi_n = \cos[\kappa_n z]e^{iky}$, where $\kappa_n = \pi/t_z$, where t_z is the film thickness. Also, form Eq. (18), one can get a dispersion relation for the magnetostatic waves in the form: $\kappa_n^2 = \mu_{yy}(\omega)k^2$. The thickness profile of a magnetostatic SW mode does not depend on its wave vector, so we can consider the transmission problem for only one magnetostatic mode.

The magnetostatic boundary conditions at an internal boundary require continuity of the tangential components of the magnetic field $\boldsymbol{H} = \nabla\psi$ (x and z components in our geometry) and of the normal component of the magnetic induction $\boldsymbol{B} = \hat{\boldsymbol{\mu}} \cdot \nabla\psi$ (y component). These conditions can be satisfied by the selection of a solution as a sum of incident, reflected and transmitted waves: $\psi(y < 0) = \cos[\kappa z](e^{ik_0 y} + Re^{-ik_0 y})$ and $\psi(y > 0) = T\cos[\kappa_n z]e^{ik_1 y}$. Then, the transmission and reflection coefficients are equal to

$$R = \frac{\mu_{yy,0}k_0 - \mu_{yy,1}k_1}{\mu_{yy,0}k_0 + \mu_{yy,1}k_1}, \quad T = \frac{2\mu_{yy,0}k_0}{\mu_{yy,0}k_0 + \mu_{yy,1}k_1}. \tag{20}$$

This solution is similar to the one obtained in the scalar exchange approximation [Eq. (6)]. The only difference is the fact, that the magnetostatic wave is sensitive to the variation of the product of a wave number by the yy component of the magnetic permeability tensor, but not sensitive to the variation of the SW wave vector alone. Another two features of this solution should be pointed out: (i) the solution of the transmission problem in the range of dipolar SWs *does not contain any localized SW modes* independently of the presence or absence of the SW polarization mismatch and (ii) there is no explicit dependence of the SW transmission coefficient on the SW polarization.

A dependence of the SW transmission coefficient on SW polarization may, however, be present implicitly in the dependence $\hat{\boldsymbol{\mu}}(\omega)$. To check this point, let us look at the case when the SW wave vectors in the regions before and after the boundary are the same, $k_0 = k_1$. From the dispersion law, it follows that this case requires $\mu_{yy,0} = \mu_{yy,1}$. Consequently, the reflected wave is absent [see Eq. (20)], and the incident wave passes fully through internal boundary. The polarization of the magnetostatic wave is given by $\boldsymbol{m} = \hat{\boldsymbol{\chi}}\nabla\psi$, i.e., the relation between the dynamic magnetization components has the form: to $m_x/m_y = \chi_{xy}/\chi_{yy} = i\omega/(\omega_H + \omega_{\mathrm{an},x})$. As it was mentioned above, the yy components of the susceptibility tensor χ_{yy} are the same in both regions, but the xy components *can be different*.

Indeed, one can easily find values of $\omega_{H,0(1)}$, $\omega_{\mathrm{an},0(1)}$ such that $\chi_{yy,0} = \chi_{yy,1}$, but $\chi_{xy,0} \neq \chi_{xy,1}$ for a certain frequency ω, see Eq. (19). Note, that this is possible not only in a specific case of biaxial anisotropy, but also can happen in a case of an uniaxial anisotropy. Thus, we can conclude, that a dipolar SWs can be *absolutely* insensitive to the variation of the SW polarization, at least in certain geometries. This is in a sharp contrast with the properties of the exchange SWs, which are *always* sensitive to the SW polarization mismatch.

Absolutely the same calculations with the similar conclusions one can made for the case when the FM waveguide is magnetized in-plane along the direction of the wave propagation $\boldsymbol{\mu} = \boldsymbol{e}_y$. The only difference is in the values of the transmission and reflection coefficients [see Eq. (20)], where $\mu_{yy} = 1$ [since $\mu_{z'z'} = 1 + \chi_{z'z'} = 1$, see Eq. (19)]. For any other directions of the waveguide static magnetization such a simple analysis can not be performed, because the SW profile across the film thickness becomes dependent on the SW wave vector, and the conditions at an internal boundary can not be satisfied using a single thickness SW mode. Therefore, in a complex magnetization geometry, the scattering into multiple thickness magnetostatic modes takes place at a boundary. In such a complex case, obviously, it would be difficult to try to isolate the effect of SW polarization mismatch in the scattering problem.

Let us now return to the initial problem of the transmission of a dipole-exchange SWs through a boundary. If an FM waveguide is sufficiently thin (of the order of 10–100 nm, depending on the material exchange length), the thickness profile of a propagating SW is maintained uniform by the exchange interaction *independently* of the static magnetization direction. Based on the above described properties of the magnetostatic waves, one can expect, that, at least in certain geometries, the SW would become insensitive to the polarization mismatch when the role of the dipolar interaction increases. To verify this hypothesis, we performed numerical simulation of Eq. (1) accounting for the dipolar interaction via the integral operator with Green's function kernel [Eq. (2)]. Equation (1) was solved using finite-difference method in the stationary mode (i.e., $\partial \boldsymbol{m}/\partial t = -i\omega \boldsymbol{m}$). The length of simulation area was chosen 10–20 times larger than SW wavelength, and the boundary conditions were set as the sum of harmonic incident and reflected waves at one boundary, and transmitted wave at other boundary, with unknown reflection and transmission rates. This approach leads, finally, to a linear equation system for the coefficients R and T and a set discretized magnetization values.

These numerical calculations showed that the above described behavior takes place if the waveguide static magnetization does not have in-plane components that are perpendicular to the SW propagation direction, $\mu_x = 0$, i.e., it takes place for perpendicular magnetization ($\boldsymbol{\mu} = \boldsymbol{e}_z$), for "backward volume waves geometry" ($\boldsymbol{\mu} = \boldsymbol{e}_y$), and for any magnetization configuration between these two. For such magnetization geometries, the SW transmission through a boundary becomes less sensitive to the polarization mismatch with the increase of the role of the dipolar interaction (this increase was simulated by the increase of the film thickness), and in the limit of a negligible exchange interaction the effect of polarization disappears completely. The same feature was pointed above in our micromagnetic simulations (see Fig. 5).

However, if $\mu_x \neq 0$, in particular, in the case of a "Damon-Eshbach geometry" ($\boldsymbol{\mu} = \boldsymbol{e}_x$), the effect of the SW polarization does not disappear completely even for the dipole-dominated SWs. In particular, the SW reflection takes place if $k_0 = k_1$, but $\boldsymbol{m}_0 \neq \boldsymbol{m}_1$. Such a drastic dependence on the direction of the static magnetization can be understood recalling the above mentioned solution of the Walker's equation. In the above considered dipolar case of perpendicular magnetization, the SW polarization is defined by the xy and yy components of the susceptibility tensor, however, the xy component of the same tensor *does not contribute* to the SW dispersion law, and, consequently, to the SW propagation and scattering. Thus the SW propagation would not be affected by the m_x component of the dynamic magnetization in the considered case. A similar situation takes place in the case of the dipole-exchange SW propagating in thin films when $\mu_x = 0$, because xx and xy components of the magneto-dipolar Green function in Eq. (1) are identically zero, $G_{xx} = G_{xy} = 0$. However, as soon as $\mu_x \neq 0$, both dynamic magnetization component have the y or/and z components, and, thus, both of them contribute to the SW propagation, since $G_{yy}, G_{zz} \neq 0$. Also, we should note, that different symmetry of dynamic magnetic fields of a SW in the Damon-Eshbach geometry leads to different SW transmission features in general, not only regarding the SW polarization [52].

Concluding this section we can state, that the effect of the SW polarization mismatch on the transmission through an internal boundary is more complex in the case of dipole-dominated SWs, compared to the case of the exchange-dominated SWs. In certain geometries ($\mu_x = 0$), this effect disappears, while in other geometries it is still present. Also, in the case of dipolar SWs the polarization difference does not lead to the formation of dipolar-dominated localized SWs. The evanescent SWs, discussed in Sec. III, are, of course, still present, because the exchange interaction requires the magnetization continuity. However, these localized SWs do not contribute to the transmission and reflection coefficients of the dipolar SWs. In the intermediate region, when both dipolar and exchange interaction are important, one should expect a smooth transition from the transmission rules for the exchange-dominated SWs to the transmission rules characteristic to the dipole-dominated SWs. In particular, one should expect a smooth disappearance of the effect of the SW polarization mismatch in the case of a static magnetization with $\mu_x = 0$. The characteristic values of the SW wave number, when this transition occurs can be obtained from the comparison of the term $\boldsymbol{m}_k^* \cdot (\hat{\boldsymbol{F}}_k - \hat{\boldsymbol{F}}_0) \cdot \boldsymbol{m}_k / A_k$ evaluating the dipolar contribution and the term $\lambda_{\text{ex}}^2 k^2$ evaluating the exchange contribution to the SW dispersion. If $\lambda_{\text{ex}}^2 k^2 \gg \boldsymbol{m}_k^* \cdot (\hat{\boldsymbol{F}}_k - \hat{\boldsymbol{F}}_0) \cdot \boldsymbol{m}_k / A_k$, one can safely neglect the dynamic dipolar interaction, and use the above developed analytical vectorial scattering theory for exchange-dominated SWs (see Sec. IV of the current paper). Otherwise a numerical solution of the full problem Eq. (1) should be used.

VI. SUMMARY

In this work, we have developed a theory of an SW transmission and reflection from a sharp internal boundary, taking into account the SW polarization. The difference in the SW polarizations before and after the boundary accompanies the difference in the SW wave numbers in almost all the cases, except some symmetric ones. However, the difference in polarizations is much more pronounced if the regions, separated by an internal boundary, differ by the value of anisotropy, as it happens in the case of a magnetoelectric (e.g., VCMA) control of the SW dispersion, or/and by the direction of anisotropy axes, as it takes place at an interface between two different

anisotropic ferromagnets. While the above presented theory was developed for an internal boundary within a single ferromagnet, assuming a constant static magnetization $\boldsymbol{M}_0$, and exchange length λ_{ex} in all the sample, it can be generalized to the case of an interface of two different ferromagnets, and one should expect qualitatively similar SW behavior at the boundary.

The SW polarization difference leads to three main effects. First, the exponentially localized (evanescent) SWs appear in the vicinity of the boundary. The appearance of these localized evanescent SW modes is a direct consequence of the necessity to satisfy the continuity conditions for the magnetization and its derivative within the whole ferromagnetic sample, which cannot be satisfied by propagating SWs only. The localized SWs are orthogonal to the propagating SWs of the same frequency, and have the localization lengths equal or smaller than the wavelength of a corresponding propagating SW. The existence of the localized modes results in the second effect—appearance of an additional phase shift for both reflected and transmitted SWs. This phase shift can be of any value $\Delta\phi \in [-\pi, \pi]$, and only for the case of a zero SW polarization mismatch it is reduced to $\Delta\phi = 0, \pi$ for the reflected SW and to $\Delta\phi = 0$ for the transmitted SW. Finally, a nonzero SW polarization mismatch $\mathcal{E}_{01}$ results in a decrease of the SW transmission coefficient and in an increase of the SW reflection coefficient. However, this effect is pronounced only for a sufficiently large polarization mismatch $\mathcal{E}_{01}$ (characteristic value depends on the difference of the SW wave numbers for the incident and transmitted SWs).

In spite of a nonzero polarization mismatch before and after a finite-length region with different magnetic parameters, an SW can pass this region resonantly, i.e., without reflection and with a transmission coefficient $|T| = 1$, if the propagation losses within that region are negligible. The conditions of the resonant transmission through a finite-length "gate" are affected by the SW polarization mismatch, and has the form $k_1 L_g + \psi = \pi n$, $n \in \mathbb{Z}$, where the additional phase $\psi = \psi(\mathcal{E}_{01})$ is the function of the polarization difference. In particular, for relatively small polarization mismatch, the phase is proportional to $\psi \sim \mathcal{E}_{01}^2$.

All these features are intrinsic for the exchange-dominated SW, since exchange interaction requires continuity of the magnetization and its derivatives. In the case of dipole-dominated SWs, the influence of SW polarization difference is not as pronounced, and can disappear completely in certain magnetization geometries.

ACKNOWLEDGMENTS

This work was supported in part by the U.S. National Science Foundation (Grants No. EFMA-1641989 and No. ECCS-1708982), by the U.S. Air Force Office of Scientific Research under the MURI Grant No. FA9550-19-1-0307, and by the Oakland University Foundation. R.V. acknowledges support from the Ministry of Education and Sciences of Ukraine (Projects No. 0115U002716 and No. 0118U004007).

[1] D. D. Stancil and A. Prabhakar, *Spin Waves. Theory and Applications* (Springer, New York, 2009).
[2] A. A. Serga, A. V. Chumak, and B. Hillebrands, J. Phys. D: Appl. Phys. **43**, 264002 (2010).
[3] V. V. Kruglyak, S. O. Demokritov, and D. Grundler, J. Phys. D: Appl. Phys. **43**, 264001 (2010).
[4] *Magnonics. From Fundamentals to Applications*, edited by S. O. Demokritov and A. N. Slavin (Springer, Berlin, 2013).
[5] *Magnetism of Surfaces, Interfaces, and Nanoscale Materials*, edited by R. E. Camley, Z. Celinski, and R. L. Stamps, Handbook of Surface Science Vol. 5 (Elsevier, Amsterdam, 2016).
[6] S. O. Demokritov, A. A. Serga, A. André, V. E. Demidov, M. P. Kostylev, B. Hillebrands, and A. N. Slavin, Phys. Rev. Lett. **93**, 047201 (2004).
[7] M. P. Kostylev, A. A. Serga, T. Schneider, T. Neumann, B. Leven, B. Hillebrands, and R. L. Stamps, Phys. Rev. B **76**, 184419 (2007).
[8] T. Neumann, A. A. Serga, B. Hillebrands, and M. P. Kostylev, Appl. Phys. Lett. **94**, 042503 (2009).
[9] U.-H. Hansen, M. Gatzen, V. E. Demidov, and S. O. Demokritov, Phys. Rev. Lett. **99**, 127204 (2007).
[10] A. A. Serga, T. Neumann, A. V. Chumak, and B. Hillebrands, Appl. Phys. Lett. **94**, 112501 (2009).
[11] M. Fiebig, J. Phys. D: Appl. Phys. **38**, R123 (2005).
[12] C.-W. Nan, M. I. Bichurin, S. Dong, D. Viehland, and G. Srinivasan, J. Appl. Phys. **103**, 031101 (2008).
[13] F. Matsukura, Y. Tokura, and H. Ohno, Nat. Nano. **10**, 209 (2015).
[14] W.-Y. Tong, Y.-W. Fang, J. Cai, S.-J. Gong, and C.-G. Duan, Comput. Mater. Sci. **112, Part B**, 467 (2016).
[15] M. Weisheit, S. Fähler, A. Marty, Y. Souche, C. Poinsignon, and D. Givord, Science **315**, 349 (2007).
[16] C.-G. Duan, J. P. Velev, R. F. Sabirianov, Z. Zhu, J. Chu, S. S. Jaswal, and E. Y. Tsymbal, Phys. Rev. Lett. **101**, 137201 (2008).
[17] S. Miwa, M. Suzuki, M. Tsujikawa, T. Nozaki, T. Nakamura, M. Shirai, S. Yuasa, and Y. Suzuki, J. Phys. D: Appl. Phys. **52**, 063001 (2018).
[18] W.-G. Wang, M. Li, S. Hageman, and C. L. Chien, Nat. Mater. **11**, 64 (2012).
[19] Y. Shiota, T. Nozaki, F. Bonell, S. Murakami, T. Shinjo, and Y. Suzuki, Nat. Mater. **11**, 39 (2012).
[20] J. Zhu, J. A. Katine, G. E. Rowlands, Y.-J. Chen, Z. Duan, J. G. Alzate, P. Upadhyaya, J. Langer, P. K. Amiri, K. L. Wang, and I. N. Krivorotov, Phys. Rev. Lett. **108**, 197203 (2012).
[21] R. Verba, M. Carpentieri, G. Finocchio, V. Tiberkevich, and A. Slavin, Sci. Rep. **6**, 25018 (2016).
[22] Y.-J. Chen, H. K. Lee, R. Verba, J. A. Katine, I. Barsukov, V. Tiberkevich, J. Q. Xiao, A. N. Slavin, and I. N. Krivorotov, Nano Lett. **17**, 572 (2017).
[23] B. Rana, Y. Fukuma, K. Miura, H. Takahashi, and Y. Otani, Appl. Phys. Lett. **111**, 052404 (2017).
[24] A. O. Leon, M. G. Clerc, and D. Altbir, Phys. Rev. E **98**, 062213 (2018).

[25] S.-S. Ha, N.-H. Kim, S. Lee, C.-Y. You, Y. Shiota, T. Maruyama, T. Nozaki, and Y. Suzuki, Appl. Phys. Lett. **96**, 142512 (2010).
[26] K. Nawaoka, Y. Shiota, S. Miwa, H. Tomita, E. Tamura, N. Mizuochi, T. Shinjo, and Y. Suzuki, J. Appl. Phys. **117**, 17A905 (2015).
[27] M. K. Niranjan, C.-G. Duan, S. S. Jaswal, and E. Y. Tsymbal, Appl. Phys. Lett. **96**, 222504 (2010).
[28] G. Rado and J. Weertman, J. Phys. Chem. Sol. **11**, 315 (1959).
[29] V. A. Ignatchenko, Fiz. Met. Metalloved. **36**, 1219 (1973).
[30] V. S. Tkachenko, V. V. Kruglyak, and A. N. Kuchko, Metamaterials **3**, 28 (2009).
[31] V. S. Tkachenko, V. V. Kruglyak, and A. N. Kuchko, Phys. Rev. B **81**, 024425 (2010).
[32] V. V. Kruglyak, O. Y. Gorobets, Y. I. Gorobets, and A. N. Kuchko, J. Phys.: Cond. Matter. **26**, 406001 (2014).
[33] K. Y. Guslienko, S. O. Demokritov, B. Hillebrands, and A. N. Slavin, Phys. Rev. B **66**, 132402 (2002).
[34] K. Y. Guslienko and A. N. Slavin, Phys. Rev. B **72**, 014463 (2005).
[35] M. Kostylev, J. Appl. Phys. **115**, 233902 (2014).
[36] P. Gruszecki, Y. S. Dadoenkova, N. N. Dadoenkova, I. L. Lyubchanskii, J. Romero-Vivas, K. Y. Guslienko, and M. Krawczyk, Phys. Rev. B **92**, 054427 (2015).
[37] V. V. Kruglyak, C. S. Davies, V. S. Tkachenko, O. Y. Gorobets, Y. I. Gorobets, and A. N. Kuchko, J. Phys. D: Appl. Phys. **50**, 094003 (2017).
[38] Y. I. Gorobets and S. A. Reshetnyak, Tech. Phys. **43**, 188 (1998).
[39] S. A. Reshetnyak, Phys. Solid State **46**, 1061 (2004).
[40] S. Mieszczak, O. Busel, P. Gruszecki, A. N. Kuchko, J. W. Kłos, and M. Krawczyk, An anomalous refraction of spin waves as a way to guide signals in curved magnonic multimode waveguides, arXiv:2001.11356 [physics.app-ph].
[41] S. V. Vasiliev, V. V. Kruglyak, M. L. Sokolovskii, and A. N. Kuchko, J. Appl. Phys. **101**, 113919 (2007).
[42] C. S. Chang, M. Kostylev, E. Ivanov, J. Ding, and A. O. Adeyeye, Appl. Phys. Lett. **104**, 032408 (2014).
[43] V. D. Poimanov and V. G. Shavrov, J. Phy.: Conf. Ser. **1389**, 012134 (2019).
[44] Q. Wang, B. Heinz, R. Verba, M. Kewenig, P. Pirro, M. Schneider, T. Meyer, B. Lägel, C. Dubs, T. Brächer, and A. V. Chumak, Phys. Rev. Lett. **122**, 247202 (2019).
[45] A. G. Gurevich and G. A. Melkov, *Magnetization Oscillations and Waves* (CRC Press, New York, 1996).
[46] R. Verba, G. Melkov, V. Tiberkevich, and A. Slavin, Phys. Rev. B **85**, 014427 (2012).
[47] R. Verba, G. Melkov, V. Tiberkevich, and A. Slavin, in *Magnetism of Surfaces, Interfaces, and Nanoscale Materials*, edited by R. E. Camley, Z. Celinski, and R. L. Stamps, Handbook of Surface Science Vol. 5, (Elsevier, Amsterdam, 2016), pp. 215–241.
[48] O. Dzyapko, I. Lisenkov, P. Nowik-Boltyk, V. E. Demidov, S. O. Demokritov, B. Koene, A. Kirilyuk, T. Rasing, V. Tiberkevich, and A. Slavin, Phys. Rev. B **96**, 064438 (2017).
[49] K. Y. Guslienko and A. N. Slavin, J. Magn. Magn. Mater. **323**, 2418 (2011).
[50] A. Vansteenkiste, J. Leliaert, M. Dvornik, M. Helsen, F. Garcia-Sanchez, and B. Van Waeyenberge, AIP Adv. **4**, 107133 (2014).
[51] D. D. Stancil, *Theory of Magnetostatic Waves* (Springer-Verlag, New York, 1993).
[52] M. Mohseni, R. Verba, T. Brächer, Q. Wang, D. A. Bozhko, B. Hillebrands, and P. Pirro, Phys. Rev. Lett. **122**, 197201 (2019).